Iranian Journal of Physics Research, Vol. 24, No. 3, 2024
DOI: 10.47176/ijpr.24.3.11791

Influence of dysprosium cation on structural and magnetic properties of thin films nickel-cobalt ferrite: using spray pyrolysis method

J Khobzade, A Avazpour*, A Modaberasl, and A Nikzad
Physics Departement, College of Sciences, Yasouj University, Yasouj, Iran

*Email: avazpour@yu.ac.ir

(Received 20 November 2023 ; in final form 28 April 2024)

Abstract
In this study, nickel-cobalt ferrite nanoparticles were prepared using spray pyrolysis. X-Ray Diffraction (XRD), Fourier Transform Infrared Spectroscopy (FTIR), and Vibration Sample Magnetometer (VSM) were used to examine the structural and magnetic properties of the obtained samples. In addition, the size, dispersion, and morphology of the particles on the surface of the glass substrate were observed and analyzed by atomic force microscope (AFM). The amount of dysprosium cation contamination was x=0.0, 0.025, 0.05, 0.075, and 1.0. All the peaks identified in the diffraction patterns of the samples were in good agreement with the reference card, and the Miller indices were indexed. FTIR spectra were obtained in the wavenumber range of 400-2000 cm^{-1}. The hysteresis loops are symmetric, and an increasing or decreasing trend of the parameters can be observed. This shows the high purity of the prepared samples without any distorted phases. In this study, the amount of magnetization (Ms) decreased, whereas an increasing trend was observed for the coercivity (Hc). The prepared magnetic nanoparticles have many applications in ferrofluids, color imaging, magnetic cooling, drug delivery, detoxification of biological fluids, and magnetic cell separation. In addition, they can be used in miniaturized inductive electric sensors, inductors, high-frequency equipment, and biotechnological applications.

Keywords: nanoparticles, magnetic properties, nickel-cobalt ferrite, spray pyrolysis

1. Introduction

Nanoscale materials exhibit different properties, and magnetic materials are no exception to this rule. Magnetic properties are strongly dependent on particle size. For example, in ferromagnetic materials, when the particle size becomes smaller than a single domain, superparamagnetic behavior occurs. Supermagnetic nanoparticles have been used in many applications, including ferrofluids, color imaging, magnetic cooling, anticancer drug delivery, biological fluid detoxification, and magnetic cell separation. Using miniaturized inductive electric sensors, three-dimensional transducers, inductors, high-frequency equipment, and biotechnological applications have been investigated [1]. Ferrites can be classified into three categories: spinels, garnets, and hexagonal ferrites. Cobalt ferrite is a candidate for high-density recording devices owing to its high coercivity, medium saturation magnetization, chemical stability, and mechanical hardness. It is inclined towards an inverted spinel structure. High-spin ions coordinated in octahedral sites exhibit strong spin-orbit (SO) coupling and produce large crystalline magneto-anisotropy [2].

$NiFe_2O_4$ is one of the most important spinel ferrites, and its properties depend on cation distribution, type of substitution, and preparation method. They have interesting properties and applications such as soft magnets and low-loss materials at high frequencies. A soft ferromagnetic material is crystallized completely in inverted spinel structures such that all nickel ions are placed in octahedral positions and iron ions occupy tetrahedral and octahedral positions [3].
Recently, composite spinel ferrites have attracted attention owing to the advantages of combining two single-phase ferrites. The production and investigation of the structural and magnetic properties of composite-structure ferrites such as nickel- zinc, magnesium-nickel, and cobalt- nickel ferrites have been reported [4]. Physical and chemical methods can be used for the synthesis of thin films. This naming depends on the layering process, the energy source, and the layering environment. Spray pyrolysis is a low-cost chemical method for coating thin layers. In addition, the layering of a wider surface can be performed using this method. This is a common and simple method for preparing thin and thick layers of oxides and binary and ternary compounds of semiconductors, insulators, magnetic materials, and

superconductors. This method has been used to prepare thin layers of transparent conductive oxides, such as nickel oxide, tin oxide, and zinc oxide.

In this study, a thin layer of nickel–cobalt ferrite doped with a cation dysprosium was constructed using the spray pyrolysis method. Since the dysprosium is the rare earth element and has a strong spin- orbit interaction, it can change the magnetic properties and increase the coercive field. In the following sections, the structural and magnetic properties of this layer are investigated.

2. Research methodology

The structural, optical, magnetic, and electrical properties of ferrites can be changed using layering methods. In this study, spray pyrolysis was used to coat samples of nickel-cobalt ferrite contaminated with cation dysprosium . Spray pyrolysis has been used to coat a wide range of materials, including ceramics, magnetics, and semiconductors. [5]. Using this method and controlling the layering conditions, regular layers with perfect crystal structures can be achieved. The coating material on a hot substrate surface can be an organic or inorganic metal solution sprayed under air pressure [6]. We used glass substrates, including KH microscopic pieces model 7105, with dimensions $24\times 75 mm^2$ and a thickness of 1 mm. All samples were prepared at a bed temperature of 450 °C with a spray rate of 5 ml/min using a dry air pressure of 3.5 bar as the carrier gas. iron chloride ($FeCl_3.6H_2O$) with molar mass of 270.30 g/mol, nickel chloride ($NiCl_2.6H_2O$) with molar mass of 237.69 g/mol, chloride Cobalt ($CoCl_2.6H_2O$) with molar mass of 237.90 g/mol, dysprosium chloride ($DyCl_3.6H_2O$) with molar mass of 376.95 g/mol, double distilled water, and sodium hydroxide (NaOH) with molar mass of 40 g/mol were used to prepare the sprayable solution samples. High-purity samples were prepared from Merck. In addition, the concentrations of the doped dysprosium cations with different ratios were considered.

First, chloride salts were dissolved in double distilled water using a magnetic stirrer and 0.1 M homogeneous solutions were prepared. Then, according to the conditions mentioned in table 1, the created layer was sprayed on the glass substrates through a nozzle with a diameter of about 8 mm and under a pressure of about 30 MPa in the air atmosphere. It should be noted that the temperature applied to all the layers that were placed on the hot surface in a rotating manner was equal to 450 °C. All the thin layers were prepared under the same conditions and as optimal as possible, and the only difference between the different layers was the concentration of the dysprosium doping cation in the samples. After the solutions were prepared, the spray pyrolysis device was prepared. The rotating hot plate was cleaned and all the paths of dry air and solution were washed and possible contaminations were removed. The X-ray diffraction (XRD) patterns of prepared $Ni_{0.7}Dy_xCo_{0.3}Fe_{2-x}O_4$ samples were carried out using Rigaku-ultra IV, Japan with monochromatic $Cu-K_\alpha$ radiation ($\lambda = 0.1541 nm$) at 30 mA and 40 kV. The diffraction data for the thin film were carried out from 20 to 70^0 of 2θ at a scan rate of 5^o/min and room temperature. Also, using Fourier transform infrared analysis (FTIR) by the instrument characteristics of Perkinelmer-spectrum two, USA, structural properties and functional groups of thin layer compositions were analyzed and investigated. In addition, the magnetic properties of prepared samples were analyzed by vibrating sample magnetometer (VSM-MDK, Iran) at room temperature and up to the maximum applied field of 10 KOe..

3. Results and discussion

The crystal size and lattice parameters changed with the doping of dysprosium cations in the ferrite structure. It should be noted that the changes do not imply a change in the crystal structure; these parameters can be reduced or increased, but the crystal structure and the pure crystal phase do not change [7]. In other X-ray diffraction patterns of the doped samples, the intensity of the peaks increased to some extent. This can be attributed to the increase in the amount of crystallization of the prepared samples during heat treatment on the surface of the glass substrate. The size of the crystals and lattice parameters of the spinel nickel-cobalt ferrites are listed in table 2. As shown in the table, the crystallite size and lattice parameter of the x = 0 sample were 36.242 Å and a=b=c= 8.349 Å, respectively. By using Scherrer's equation (eq. (1)), and eq. (2), the crystallite size (D) and the lattice parameters were calculated [8]

$$D=k\lambda/\beta\cos\theta, \quad (1)$$

Where k, β and λ are the Scherer's constant, the diffraction peak width at the half maximum, and the wavelength of X-ray source , respectively [8]

$$\frac{1}{d^2}=\frac{(h^2+k^2+l^2)}{a^2} \quad , \quad (2)$$

where d is the distance between the crystal planes, h, k, and l are the Miller indices, and a is the lattice parameter. With the first amount of dispersium cation doping in the nickel-cobalt ferrite composition structure, the crystallite size reached 37.442 Å and the lattice parameter reached a=b=c=8.362 Å. When x=0.10, the crystallite size and lattice parameters changed to 38.264 and 8.388 Å, respectively. This can be attributed to the difference of radius of dysprosium cation (0.99 Å) comparing with that of Fe cation (0.64 Å).

Table 1 shows the coating layer on the glass substrate under an air pressure of approximately 30 MPa in air atmosphere. The X-ray diffraction patterns of the prepared samples are shown in figure 1. Using X-ray diffraction analysis, it was possible to identify the phases of the prepared samples. As demonstrated in figure 1, the diffraction peaks of $Ni_{0.7}Co_{0.3}Fe_2O_4$ at 2θ correspond to the (220), (311), (222), (400), (422), (511), and (440) crystal planes.

Table 1. Spray conditions of nickel-cobalt ferrite samples contaminated with dysprosium cation with chemical formula $Ni_{0.7}Dy_xCo_{0.3}Fe_{2-x}O_4$ for x=0.00, 0.025, 0.050, 0.075 and 0.100.

Sample	Substrate Temperature (°C)	Solution volume (ml)	Nozzle height (cm)	Spray rate (ml/min)
x=0.00	450	150	40	5
x=0.025	450	150	40	5
x=0.050	450	150	40	5
x=0.075	450	150	40	5
x=0.100	450	150	40	5

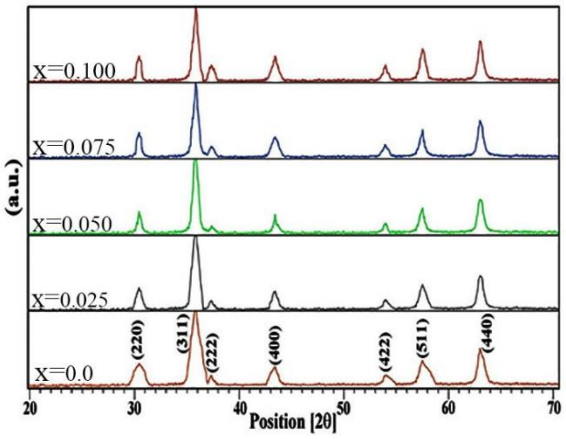

Figure 1. Patterns of X-ray diffraction of samples prepared with dispersed cation.

The peaks identified in the diffraction pattern of the samples were in full agreement with the JCPDS reference card 003-0875 and the Miller indices corresponding to each peak were also indexed. With the doping of the dysprosium cation, there was no change in the crystalline structure of ferrite, and no impurity phases or secondary phases were observed in any pattern.

Infrared Fourier transform spectra in the range of 400-2000 cm^{-1} are shown in figure 2. This range covers the metal-oxygen bonds and functional groups of the minerals. Two characteristic peaks of spinel ferrites were created in the wavenumber range of 400-650 cm^{-1}, which are the main characteristics of iron oxide structures and spinel ferrites [9]. Therefore, the material was produced at wavenumbers of 468 cm^{-1} and 625 cm^{-1} [10].

The doped cation creates a special oxygen-metal bond with the dispersed cation (Dy–O) that appears in the waveform at 548 cm^{-1}. With an increase in cation doping, more intensity was created at this wavenumber [10]. The slight changes in the positions of different bonds could be due to changes in the distance between different oxygen and metal bonds (Fe–O, Ni–O, Co–O, and Dy–O) in different compounds.

Table 2. Lattice parameters and crystallite size of prepared samples from X-ray diffraction patterns.

Sample	*D* (Å)	*a=b=c* (Å)
x =0.00	36.242	8.349
x =0.025	36.984	8.352
x =0.050	37.442	8.362
x =0.075	37.862	8.374
x =0.100	38.264	8.388

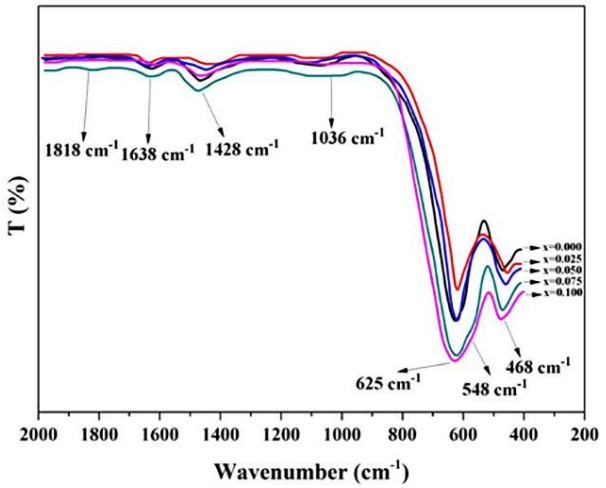

Figure 2. Fourier transform infrared spectra in the range of 400-2000 cm^{-1} wavenumbers for different values of dysprosium cation doping.

The characteristic wavenumber created at 468 cm^{-1} represents tetrahedral inter-lattice sites between metal and oxygen in the structure, and the characteristic wavenumber bonds created at 625 cm^{-1} also represent octahedral inter-lattice sites between metal and oxygen in the structure [11]. The tetrahedral and octahedral inter-lattice sites change in the wave ranges 390-525 cm^{-1} and 630-560 cm^{-1}, respectively. The peaks at 1036 cm^{-1} are related to the dominant metal-oxygen bonds, which are related to iron cations (Fe–O). It should be noted that this peak appeared at high temperatures [10].

Figure 3 shows two-dimensional atomic force microscope (AFM) images of all prepared samples. From these two-dimensional images, the size, the amount of dispersion, and the morphology of the particles on the surface of the glass substrate can be observed and analyzed. The particle size was analyzed with Image j software and the average particle size for the nickel-cobalt ferrite sample was found to be 88 nm. With the first doping of dysprosium cation in the structure of the composition, the average particle size changed slightly and was equal to 90 nm. In the next step, by increasing the amount of dysprosium cation in the ferrite structure, the particles strongly adhered to each other and formed a complete layer on the substrate. Also, in this case, the particles had an approximate rod growth and the density of the particles increased.

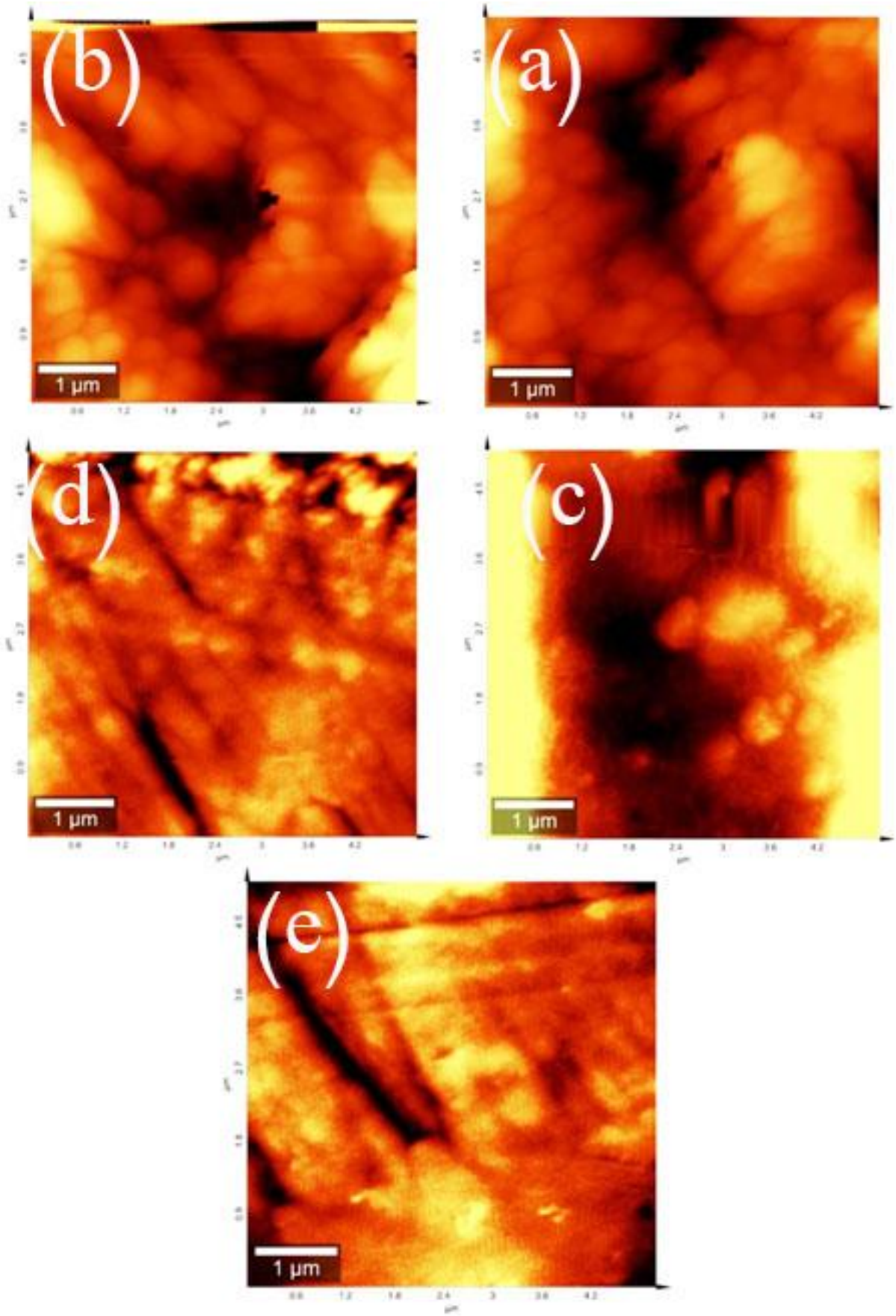

Figure 3. 2-dimensional AFM images of all prepared samples.

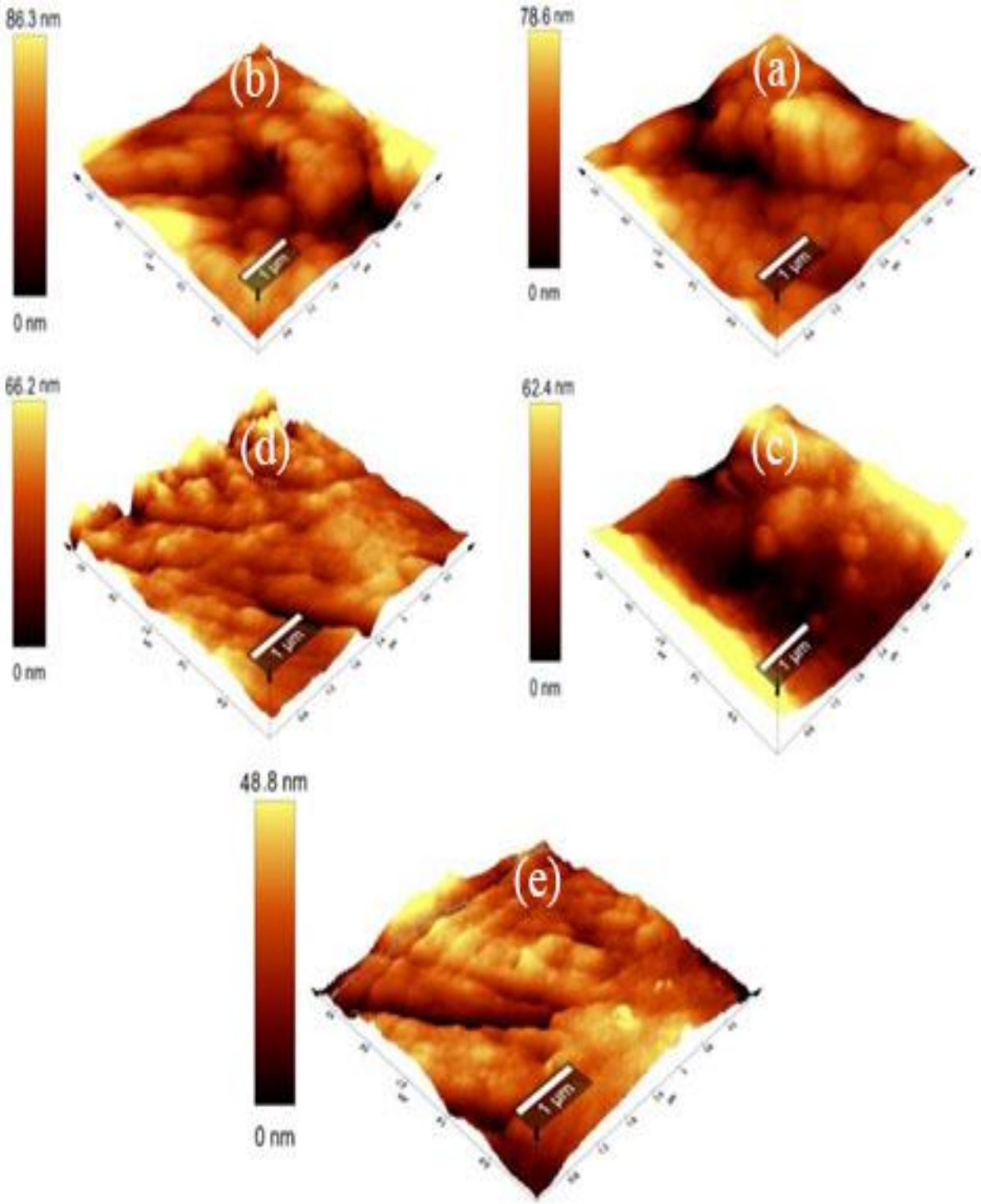

Figure 4. 3-dimensional AFM images of all prepared samples.

In the next stages, by increasing the dysprosium cation, the coating layer on the substrate was obtained in a smoother and more uniform manner, and at the same time, the growth of the particle size was higher. So, for the final composition (x=0.10), the average particle size was equal to 120 nm. The increase in the particle sizes can be due to the placement of the doped cation in the grain boundary, which has led to the formation of welds between the grain boundaries and the adhesion of the particles to each other. The adhesion of the particles to each other can be due to the magnetic and nanoscale of the particles during spraying and heat treatment on the surface of the glass substrate. Figure 4 shows three-dimensional atomic force microscope images of all prepared samples. These images are exactly the three-dimensional mode of the two-dimensional images seen in figure 3. Three-dimensional images of a certain area of the thin layer can show the topography of the layers. By the increase of doping, the layers have gradually become more orderly and regular and more uniform layers have been created.

Table 3. Magnetic parameters of samples prepared for different doped cation values.

$Ni_{0.7}Dy_xCo_{0.3}Fe_{2-x}O_4$	*Hc* (Oe)	*Mr* (emu/cm^3)	*Ms* (emu/cm^3)
x = 0.000	20	86	468
x = 0.025	46	74	424
x = 0.050	66	66	388
x = 0.075	84	56	352
x = 0.100	168	36	324

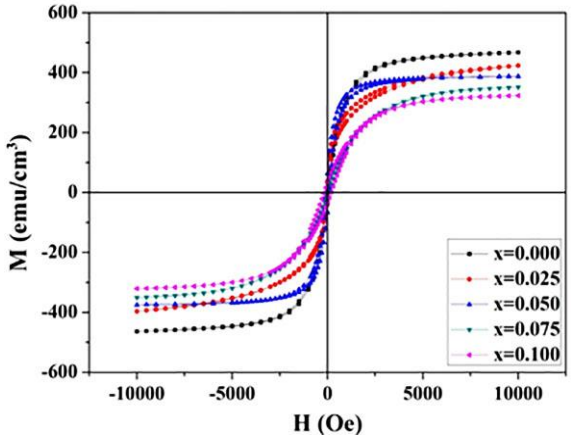

Figure 5. Magnetic hysteresis loop of all samples for different doped cation values.

The magnetic hysteresis loops of the prepared samples are shown in figure 5. The analysis was performed at room temperature up to the maximum applied magnetic field of 10 KOe. The saturation magnetization (Ms), residual magnetization (Mr), and coercive force (Hc) parameters are presented in table 3. According to figure 5, the hysteresis loops are symmetrical and the increase or decrease of parameters is observable. The high purity of samples without the disturbing phases are indicated. The magnetization has been decreasing while coercivity is increasing. The saturation magnetization for combination x = 0.00 was 468 emu/cm^3 and the residual magnetization value was 86 emu/cm^3. For this compound, the coercivity was equal to 20 Oe and showed that the soft magnetic phase was dominant. Increasing the amount of dysprosium doped cations in the structure for x = 0.05 composition, led to a decrease in the saturation magnetization (388 emu/cm^3) and residual magnetization (66 emu/cm^3) and an increase in the coercivity up to 66 Oe. This process continued up to the x = 0.10 composition and reached 324 emu/cm^3, 36 emu/cm^3, and 168 Oe for saturation magnetization, residual magnetization, and coercivity, respectively. Magnetization and coercivity depend on several factors such as chemical composition, material preparation method, coating method, substrate temperature, type and amount of doped cation, surface properties, and particle size. As mentioned above, with increasing of dysprosium cation in nickel-cobalt ferrite structure, magnetization has been decreased. This can be due to the decrease in the total magnetic moment of the lattice due to the doping of the dysprosium cation in the structure. By doping the cation in the structure, the stoichiometry is changed and the lattice is distorted, which in turn leads to a change in the lattice's hyper-exchange interactions [12-14].

The magnetic moment of iron cation as a ferromagnetic element is equal to 5 μ_B. This cation has been doped in combination with the dysprosium cation for different amounts. Also, dysprosium cation is a paramagnetic material. Therefore, the superexchange interactions between the octahedral and tetrahedral sites in the network have decreased and have resulted in the reduction of the compound magnetization. The coercivity has been increased by increasing the doped cation from 20 Oe for composition of x=0.0 to 168 Oe for composition x = 0.10. Since the dysprosium is the rare earth element and has a strong spin- orbit interaction, it can increase the coercive field. In addition, the coercivity is dependent on surface effects, lattice defects, magnetic anisotropies and particle size. By doping Dy cations instead of Fe cations in the structure, lattice defects have been created in the ferrite structure. Since the prepared materials were in the form of thin layers, shape anisotropy played a greater role than other anisotropies such as crystal anisotropy.

The increase in grain boundaries has made the movement of magnetic moments more difficult and has led to an increase in the coercivity [15-17].

4. Conclusion

In this study, thin films of $Ni_{0.7}Dy_xCo_{0.3}Fe_{2-x}O_4$ were prepared by spray pyrolysis at 450 °C with different values of doping. X-ray diffraction patterns of samples with and without dysprosium cation doping showed that all the samples were single-phase, and in the nickel–cobalt composition, there were no impurity phases. In addition, secondary and interfering phases are not observed in the diffraction patterns. These results indicated the success of the doping. The Fourier transform spectra of the samples were obtained in the wavenumber range of 400- 2000 cm^{-1}. The characteristic peaks of spinel ferrites occur in the wavenumber of 400 cm^{-1} to 600 cm^{-1}. The peak value of the lower wavenumber is attributed to the vibrations of the tetrahedral interlattice sites, and the peak of the wavenumber is attributed to the vibrations of the octahedral interlattice sites. The atomic force microscopy images show that the morphology features changes with the increase of dysprosium-doping concentration and a denser microstructure and smoother surface obtained. By performing vibrational sample magnetometer analysis, a decreasing trend for magnetization and an increasing trend for the magnetization residue were obtained. The magnetization decreased from 468 emu/cm^3 to 324 emu/cm^3, and the residual magnetization decreased from 86 emu/cm^3 to 36 emu /cm^3. The coercivity was increased from 20 to 168 Oe. The sample was transformed into a magnetically soft sample by doping cations in the ferrite structure. Magnetic nanoparticles have many applications, such as ferrofluids, color imaging, magnetic refrigeration, controlled drug delivery, and detoxification of biological fluids. In addition, they can be used in miniaturized induction electricity sensors, inductors, high-frequency equipment, and biotechnological applications.

References

1. R C Kambale, et al., *J. Appl. Phys*. (2011) 1.
2. I H Dunn, S E Jacobo, and P G Bercoff, *J. Alloys Compd*. **691** (2017) 130.
3. D H Chen and X R He, *J. Mater. Res. Bull*. **36** (2001)1369.
4. L Chauhan and N Singh, *J. Ceram. Int*. **43**, 11 (2017) 8378.
5. H Kamal, et al., *J. Cryst. Growth* **262** (2004) 424.
6. H Kamal, et al., *Tin Solid Films* **483** (2005) 330.
7. V Manikandan, et al., *J. Mol. Struct*. **1177** (2019) 485.
8. D K Pawar, et al., *J. Alloys Compd*. **509**, 8 (2011) 3587.
9. A Takayama, M Okuya, and S Kaneko, *J. Solid State Ion*. **172**, 1-4 (2004) 257.
10. S M Chavan, et al., *J. Alloys Compd*. **507**, 1 (2010) 21.
11. G Dixit, et al., *J. Adv. Mater. Lett*. **3**, 1 (2012) 21.
12. A R Chavan, et al., *J. Alloys Compd*. **735** (2018) 2287.
13. P Rajagiri, et al., *J. Magn. Magn. Mater*. **499** (2020) 166200.
14. A B Mugutkar, et al., *J. Rare Earths* **38**, 10 (2020) 1069.
15. C D Lokhande, S S Kulkarni, and R S Mane, *Ceram. Int*. **37**, 8 (2011) 3357.
16. H Liu, et al., *Ceram. Int.* **47**, 1 (2021) 1318.
17. R Ade and Y S Chen, *J. Magn. Magn. Mater*. **496** (2020) 165956.